Inorganic Chemistry
Article

Inorg. Chem. **2009**, *48*, 7667–7678 **7667**
DOI: 10.1021/ic9005955

Mechanistic Investigations of the Reaction of an Iron(III) Octa-Anionic Porphyrin Complex with Hydrogen Peroxide and the Catalyzed Oxidation of Diammonium-2,2′-azinobis(3-ethylbenzothiazoline-6-sulfonate)

Ariane Brausam, Siegfried Eigler, Norbert Jux, and Rudi van Eldik*

Department of Chemistry and Pharmacy, University of Erlangen-Nürnberg, Egerlandstrasse 1, 91058 Erlangen, Germany

Received March 27, 2009

A detailed study of the effect of pH, temperature, and pressure on the reaction of hydrogen peroxide with $[Fe^{III}(P^{8-})]^{7-}$, where P^{8-} represents the octa anionic porphyrin, was performed using stopped-flow techniques. Depending on the pH, different high valent iron-oxo species were formed. At pH < 9 formation of a two-electron oxidized species [(porphyrin$^{+\bullet}$)Fe^{IV}=O] was observed. In contrast, at pH > 9 only the one electron oxidized species [(porphyrin)Fe^{IV}=O] was found to be present in solution. Under selected conditions at pH 8 it was possible to determine rate constants for both the coordination of hydrogen peroxide and subsequent heterolytic cleavage of the O−O bond. At pH 11 a composite rate constant for coordination of H_2O_2 and homolytic cleavage of the O−O bond could be measured. In addition, it was possible to determine the activation parameters for the overall reaction sequence leading to the formation of [(porphyrin)Fe^{IV}=O]. Careful analysis of the obtained data supports an associatively activated mechanism for the coordination of hydrogen peroxide. The catalytic properties of $[Fe^{III}(P^{8-})]^{7-}$ in the presence of H_2O_2 were also investigated. Both high valent iron-oxo species turned out to be able to oxidize diammonium-2,2′-azinobis(3-ethylbenzothiazoline-6-sulfonate) (ABTS) to the radical cation $ABTS^{+\bullet}$. At higher hydrogen peroxide concentrations a reduced yield of $ABTS^{+\bullet}$ was observed because of increased catalase activity of $[Fe^{III}(P^{8-})]^{7-}$. At high pH disproportionation of $ABTS^{+\bullet}$ to ABTS and $ABTS^{2+}$ occurred, which could be suppressed by an excess of unreacted ABTS. In slightly basic to acidic solutions this reaction did not play a role.

Introduction

Heme-containing peroxidases, oxygenases, and cytochrome P450 enzymes are capable of oxidizing a wide range of different substrates.[1,2] High-valent iron oxo species are thought to be the key reactive intermediates responsible for enzymatic oxidation reactions. Inspired by these enzymatic processes, various biomimetic models were developed for the catalytic oxidation of organic substrates such as alkanes and olefins.[3−7] A straightforward way to produce high-valent iron-oxo species is to use oxidants such as *m*-chloroperoxybenzoic acid, iodosylbenzene, organic peroxides, or hydrogen peroxide for the oxidation of the iron porphyrin precursor.[6,8−12] The most desirable oxidant, beside dioxygen, is hydrogen peroxide since it is cheap and environmentally friendly. Provided that a peroxide is used, prior to the formation of the iron-oxo species, coordination of peroxide takes place leading to an iron-peroxo complex [(porphyrin)Fe^{III}−OOR]. This species can either undergo heterolytic or homolytic cleavage of the O−O bond. Depending on the reaction conditions, nature of the porphyrin and oxidant, axial ligation of the iron center and solvent, either the two-electron oxidized iron(IV) oxo porphyrin radical cation complex, [(porphyrin$^{+\bullet}$)Fe^{IV} = O], or the one-electron

*To whom correspondence should be addressed. E-mail: vaneldik@chemie.uni-erlangen.de.

(1) Sono, M.; Roach, M. P.; Coulter, E. D.; Dawson, J. H. *Chem. Rev.* **1996**, *96*, 2841–2887.
(2) Meunier, B.; de Visser, S. P.; Shaik, S. *Chem. Rev.* **2004**, *104*, 3947–3980.
(3) *Metalloporphyrins in Catalytic Oxidations*.; Sheldon, R. A., Ed.; M. Dekker: New York, 1994; p 390.
(4) Meunier, B. *Chem. Rev.* **1992**, *92*, 1411–1456.
(5) McLain, J. L.; Lee, J.; Groves, J. T. *Biomimetic Oxid. Catal. Transition Met. Complexes* **2000**, 91–169.
(6) Nam, W.; Park, S.-E.; Lim, I. K.; Lim, M. H.; Hong, J.; Kim, J. *J. Am. Chem. Soc.* **2003**, *125*, 14674–14675.
(7) Hessenauer-Ilicheva, N.; Franke, A.; Meyer, D.; Woggon, W.-D.; van Eldik, R. *J. Am. Chem. Soc.* **2007**, *129*, 12473–12479.
(8) Song, W. J.; Sun, Y. J.; Choi, S. K.; Nam, W. *Chem. Eur. J.* **2005**, *12*, 130–137.
(9) Machii, K.; Watanabe, Y.; Morishima, I. *J. Am. Chem. Soc.* **1995**, *117*, 6691–6697.
(10) Yamaguchi, K.; Watanabe, Y.; Morishima, I. *J. Am. Chem. Soc.* **1993**, *115*, 4058–4065.
(11) Zipplies, M. F.; Lee, W. A.; Bruice, T. C. *J. Am. Chem. Soc.* **1986**, *108*, 4433–4445.
(12) Bruice, T. C. *Acc. Chem. Res.* **1991**, *24*, 243–249.

Published on Web 07/14/2009

oxidized iron(IV) oxo species, [(porphyrin)$Fe^{IV}=O$], is produced.[13,14] Both species are thought to be active oxidants.

An approved method to test for peroxidase activity is the color reaction of the diammonium-2,2′-azinobis(3-ethylbenzothiazoline-6-sulfonate) (ABTS).[15] ABTS is used as a trapping agent for the formed high-valent iron-oxo species.[11,16−18] Especially at higher pH, not only ABTS acts as a substrate but also hydrogen peroxide can be oxidized by the high valent iron-oxo species, yielding oxygen and water (catalase activity).[11,16]

In this study the reactivity of an octa-anionic, non μ-oxo dimer forming, and water-soluble Fe^{III} porphyrin toward hydrogen peroxide was investigated to obtain more information on the mode of O−O bond cleavage in the corresponding iron-peroxo complex. This particular complex was selected on the basis of our earlier mechanistic studies dealing with the activation of NO by a series of water-soluble, non μ-oxo dimer forming Fe^{III} porphyrin complexes, for which water exchange kinetics and the reversible binding of NO were studied as a function of temperature, pressure, and pH.[19,20] Furthermore, our recent experience with the in situ spectroscopic identification of the possible reactive intermediates mentioned above[7,21−23] has improved our mechanistic insight into such catalytic processes and encouraged us to study the more demanding activation of hydrogen peroxide in aqueous solution. It is in general known that the aggressive nature of hydrogen peroxide often leads to unwanted decomposition reactions of porphyrin complexes and can complicate the mechanistic analysis substantially. A series of studies performed in our laboratories on closely related porphyrin complexes showed that the selected octa-anionic porphyrin complex is particularly suitable to study the activation of hydrogen peroxide and the oxidation of a model substrate in much detail.

Since pH has a significant influence on the reactivity of porphyrins in water, a wide range of pH values was covered in the present study. Furthermore, temperature and pressure dependent kinetic measurements were performed under a wide range of experimental conditions. To test the pH dependent catalytic activity of the octa-anionic porphyrin, a peroxidase assay, namely, oxidation of ABTS, was used.

Experimental Section

Materials. The water-soluble octa anionic porphyrin $Na_7[(P^{8-})Fe^{III}]$, where P^{8-} = 5^4,10^4,15^4,20^4-tetra-*tert*-butyl-5^2,5^6,15^2,15^6-tetrakis[2,2-bis(carboxylato)ethyl]-5,10,15,20-tetraphenylporphyrin, was synthesized and characterized as described in a previous paper.[19] $NaClO_4$ (Aldrich) was used to adjust the ionic strength. The employed buffers, namely, 3-(cyclohexylamino)propansulfonic acid (CAPS), [tris(hydroxymethyl)methyl]amino-propansulfonic acid (TAPS), and bis(2-hydroxyethyl)amino-tris(hydroxymethyl)methan (Bis-Tris) were purchased from Roth. Throughout the study a total buffer concentration of 0.02 M was applied. NaOH (Acros Organics) or $HClO_4$ (Fluka) were used to adjust the pH of the buffer solutions. Diammonium-2,2′-azinobis-(3-ethylbenzthiazolin-6-sulfonate) (ABTS) was used as a substrate for the oxidation reactions. Solutions of H_2O_2 were prepared by dilution of a 35% stock solution of H_2O_2 (Acros Organics). To verify the reproducible concentration of the H_2O_2 stock solution, kinetic measurements were performed regularly at a fixed H_2O_2 concentration throughout the study. No changes in the values of the rate constants were observed, from which it was concluded that the concentration of H_2O_2 remained constant throughout the measurements. All chemicals were of the highest quality commercially available and used without further purification. All solutions were prepared with deionized water.

Instrumentation. UV/vis spectra and slower kinetic runs were recorded on a Cary 5G UV/vis-NIR spectrophotometer. Time resolved UV−vis spectra were recorded with a Hi-Tech SF-3F low-temperature stopped-flow unit (Hi-Tech Scientific) equipped with a J&M TIDAS 16/300−1100 diode array spectrophotometer (J&M). Kinetic simulations were performed with the use of Specfit, Global Analysis System, version 3.0.28. Kinetic measurements at a single wavelength were performed with a thermostatted (±0.1 °C) SX-18 MV (Applied Photophysics) stopped-flow spectrometer. Absorbance changes were recorded at 405 and 488 nm.

Stopped-flow experiments at pressures up to 130 MPa were performed on a custom built instrument described before.[24,25] Kinetic traces were recorded on an IBM-compatible computer and analyzed with the OLIS KINFIT (Bogart, GA, 1989) set of programs. All kinetic measurements were performed under pseudo-first-order conditions, that is, at least a 10-fold excess of hydrogen peroxide compared to $Fe^{III}(P^{8-})$ was employed. Reported rate constants are the mean values from at least five kinetic runs.

pH measurements were performed on a Metrohm 632 pH meter equipped with a Mettler Toledo InLab 422 glass electrode, which was filled with NaCl instead of KCl to prevent precipitation of $KClO_4$. Oxygen evolution was followed with a WTW precision oxygen meter Oxi 91 equipped with an EO 90 oxygen elelctrode.

Results and Discussion

The speciation of $Fe^{III}(P^{8-})$ (Figure 1) in water is well-known from a previous study.[19] On the basis of UV−vis, ^{1}H NMR, and ^{17}O NMR data it could be concluded, that the employed octa anionic porphyrin exists as a six-coordinate diaqua species **1-H_2O** at pH < 8, whereas at pH > 10 mainly the five-coordinate monohydroxo species **1−OH** is present in solution. Up to pH 13 there was no evidence found for the formation of μ-oxo bridged dimers. UV−vis and ^{1}H NMR data give a pK_a of 9.26 ± 0.01[19] for the acid base equilibrium described below (eq 1). Negatively charged meso substituents increase the electron density at the iron center and therefore

(13) Nam, W.; Jin, S. W.; Lim, M. H.; Ryu, J. Y.; Kim, C. *Inorg. Chem.* **2002**, *41*, 3647–3652.
(14) Song, W. J.; Ryu, Y. O.; Song, R.; Nam, W. *J. Biol. Inorg. Chem.* **2005**, *10*, 294–304.
(15) Puetter, J.; Becker, R. *Methods Enzym. Anal.* (*3rd Ed.*) **1983**, *3*, 286–293.
(16) Bruice, T. C.; Zipplies, M. F.; Lee, W. A. *Proc. Natl. Acad. Sci. U.S.A.* **1986**, *83*, 4646–4649.
(17) Ozaki, S.-i.; Ishikawa, Y. *React. Kinet. Catal. Lett.* **2006**, *89*, 21–28.
(18) Eulering, B.; Schmidt, M.; Pinkernell, U.; Karst, U.; Krebs, B. *Angew. Chem., Int. Ed. Engl.* **1996**, *35*, 1973–1974.
(19) Jee, J.-E.; Eigler, S.; Hampel, F.; Jux, N.; Wolak, M.; Zahl, A.; Stochel, G.; van Eldik, R. *Inorg. Chem.* **2005**, *44*(22), 7717–7731.
(20) Franke, A.; Roncaroli, F.; van Eldik, R. *Eur. J. Inorg. Chem.* **2007**, 773–798.
(21) Wolak, M.; van Eldik, R. *Chem. Eur. J.* **2007**, *13*, 4873–4883.
(22) Franke, A.; Fertinger, C.; van Eldik, R. *Angew. Chem., Int. Ed.* **2008**, *47*, 5238–5242.
(23) Ivanovic-Burmazovic, I.; van Eldik, R. *Dalton Trans.* **2008**, 5259–5275.
(24) van Eldik, R.; Palmer, D. A.; Schmidt, R.; Kelm, H. *Inorg. Chim.* **1981**, *50*, 131–135.
(25) van Eldik, R.; Gaede, W.; Wieland, S.; Kraft, J.; Spitzer, M.; Palmer, D. A. *Rev. Sci. Instrum.* **1993**, *64*, 1355–1357.

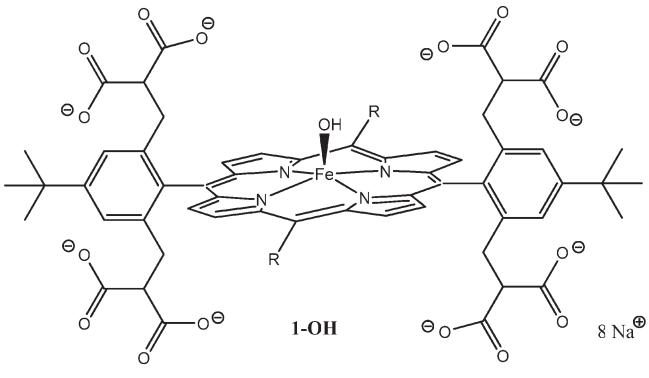

Figure 1. Schematic presentation of $Fe^{III}(P^{8-})OH$, **1−OH**.

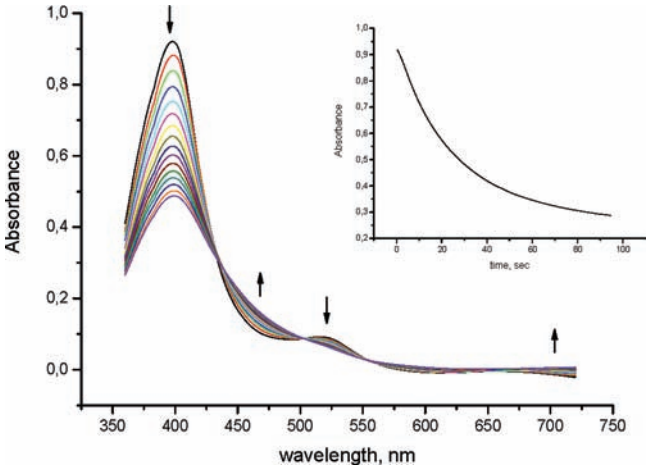

Figure 2. Spectral changes observed during the reaction of **1-H_2O** with hydrogen peroxide. Experimental conditions: [**1-H_2O**] = 1×10^{-5} M, $[H_2O_2] = 2 \times 10^{-4}$ M, pH 8 (0.02 M TAPS buffer), I = 0.2 M ($NaClO_4$), T = 4 °C, reaction time 30 s. Inset: Kinetic trace at 398 nm.

give rise to this unusual high pK_a value, compared to other water-soluble porphyrins.[26−29]

$$Fe^{III}(P^{8-})(H_2O)_2 \rightleftarrows Fe^{III}(P^{8-})(OH) + H_3O^+ \qquad pK_a \quad (1)$$

Since the ^{1}H NMR chemical shift of the β-pyrrole proton resonances is an excellent probe to determine the spin state of an iron(III) center, it could be concluded from a chemical shift of $\delta = 83$ ppm for these protons that at pD 11 the pure high spin ($S = 5/2$) monohydroxo form **1−OH** predominates. At pD 7 a chemical shift of $\delta = 47$ ppm for the β-pyrrole protons suggests an admixed $S = 3/2$, 5/2 spin system for the diaqua complex $Fe^{III}(P^{8-})(H_2O)_2$, with two weak field H_2O ligands.

From temperature- and pressure-dependent ^{17}O NMR studies at pH 7 it is known that **1-H_2O** undergoes a rapid water-exchange reaction ($k_{ex} = 7.7 \times 10^6$ s^{-1} at 25 °C).[19] As for various other porphyrins,[30] a dissociative mechanism

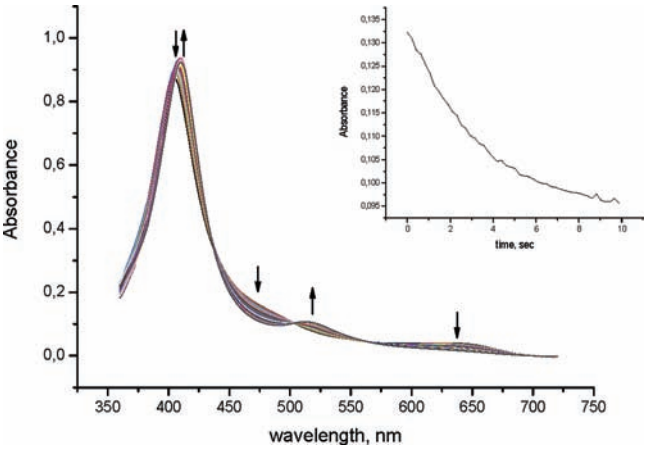

Figure 3. Spectral changes observed during the reaction of **1−OH** with hydrogen peroxide. Experimental conditions: [**1−OH**] = 1×10^{-5} M, $[H_2O_2] = 2 \times 10^{-4}$ M, pH 11 (0.02 M CAPS buffer), I = 0.2 M ($NaClO_4$), T = 4 °C, reaction time 10 s. Inset: Kinetic trace at 488 nm.

(I_d or D) with significantly positive values for $\Delta S^{\ddagger}$ (+ 91 ± 23 J mol^{-1} K^{-1}) and $\Delta V^{\ddagger}$ (+7.4 ± 0.4 cm^3 mol^{-1}) for the water exchange reaction was found.

Reactivity of $(P^{8-})Fe^{III}(H_2O)_2$ and $(P^{8-})Fe^{III}(OH)$ toward Hydrogen Peroxide. The reaction of $(P^{8-})Fe^{III}(H_2O)_2$ with hydrogen peroxide in water was followed using rapid scan spectroscopy at 4 °C. The nature of the reaction products turned out to be pH sensitive. Upon addition of hydrogen peroxide to **1-H_2O** in a buffered solution at pH < 9 the appearance of a product with a Soret band at 398 nm and a band of low-intensity with a maximum around 675 nm is observed. Spectral changes are accompanied by isosbestic points at 440, 505, and 550 nm (Figure 2). The spectral features[7,21,31] can clearly be assigned to the formation of an oxo-iron(IV)-porphyrin radical cation species [(porphyrin$^{+\bullet}$)Fe^{IV}=O], the two-electron oxidized form of **1** (abbreviated as **1**$^{+\bullet}$ in the following). In contrast, at pH > 9 a completely different spectral pattern appeared. Clean isosbestic points at 480, 500, and 550 nm are accompanied by a red-shifted Soret band at 408 nm and a low-intensity band at 525 nm, which can be assigned to the formation of an oxo-iron(IV)-phorphyrin species [(porphyrin)Fe^{IV}=O], the one-electron oxidized from of **1−OH** (abbreviated as **1**$^+$) (Figure 3). These two oxo-iron(IV) species are not

(26) Ivanca, M. A.; Lappin, A. G.; Scheidt, W. R. *Inorg. Chem.* **1991**, *30*, 711–718.
(27) Reed, R. A.; Rodgers, K. R.; Kushmeider, K.; Spiro, T. G.; Su, Y. O. *Inorg. Chem.* **1990**, *29*, 2881–2883.
(28) La, T.; Miskelly, G. M. *J. Am. Chem. Soc.* **1995**, *117*, 3613–3614.
(29) La, T.; Miskelly, G. M.; Bau, R. *Inorg. Chem.* **1997**, *36*, 5321–5328.
(30) Schneppensieper, T.; Zahl, A.; van Eldik, R. *Angew. Chem., Int. Ed.* **2001**, *40*, 1678–1680.
(31) Fujii, H. *J. Am. Chem. Soc.* **1993**, *115*, 4641–4648.

Scheme 1. Reaction of **1-H_2O** with Hydrogen Peroxide

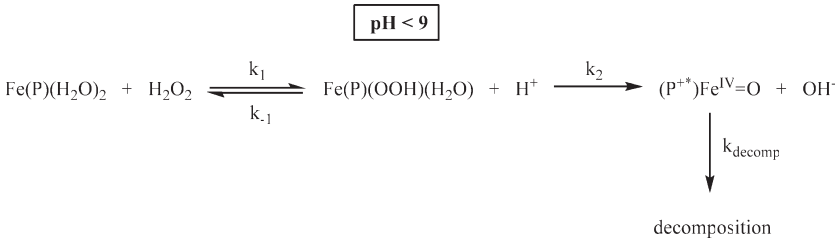

stable under the applied conditions and spontaneous degradation is observed. At lower pH values where $\mathbf{1}^{+\bullet}$ is formed, complete destruction of the porphyrin (indicated by a broadening and complete loss of intensity of the Soret band) takes place within 10 min at 4 °C, also at low hydrogen peroxide concentrations. The iron(IV)-oxo species could not be stabilized at lower temperature. In a methanol/water mixture (70:30) at −20 °C the same behavior was observed. Also $\mathbf{1}^{+}$ degrades under the applied reaction conditions, finally resulting in the destruction of the porphyrin. Only high hydroxide concentrations (pH > 12) have a certain stabilizing effect on $\mathbf{1}^{+}$, but slow decomposition of the iron(IV)-oxo species is still observed.

All kinetic data were obtained using different stopped-flow techniques under pseudo-first-order conditions, using at least a 10-fold excess of H_2O_2 compared to **1**. Since decomposition of the oxo-iron(IV)-radical cation species always interferes at pH < 9, the best results were obtained by fitting the kinetic data in the following way: The obtained spectra were cut in a way that the isosbestic point around 450 nm was only slightly blurred and subsequently fitted using a three-exponential function, where k_1 represents the formation of an iron(III)-hydroperoxo species, k_2 represents formation of $\mathbf{1}^{+\bullet}$ and k_{decomp} represents the decomposition of $\mathbf{1}^{+\bullet}$ (Scheme 1). The obtained rate constant for the decomposition of $\mathbf{1}^{+\bullet}$ was not interpreted, but the three-exponential function was necessary to obtain good fits for the kinetic traces. At pH 8 reasonable values for both k_1 and k_2 could be obtained, even though the absorbance change for the first step was very small. During the first second of the reaction a change in the slope of the kinetic traces could be observed, clearly indicating a two-step process. Furthermore, the first spectrum of the rapid scan measurement taken after 1 s could be assigned to an iron(III)-hydroperoxo species on the basis of the increase in intensity of the Soret band[22] (see Supporting Information, Figure S1). At lower pH values it was essential to perform kinetic simulations with the use of the Specfit Global Analysis program. When kinetic traces were recorded only at a single wavelength, the obtained fits and rate constants were not satisfactory to be considered in the kinetic analysis.

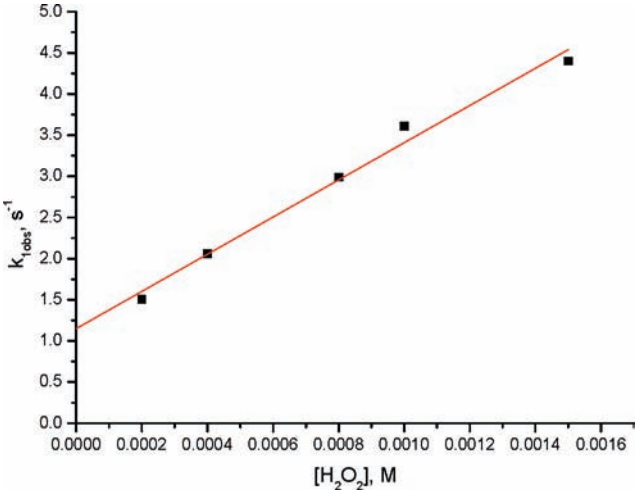

Figure 4. Plot of k_{1obs} vs $[H_2O_2]$ for the reaction of **1-H_2O** with hydrogen peroxide. Experimental conditions: [**1-H_2O**] = 1×10^{-5} M, pH 8 (0.02 M TAPS buffer), I = 0.2 M ($NaClO_4$), T = 4 °C.

It can be seen from Figure 4 that k_{1obs} depends linearly on $[H_2O_2]$ at pH 8 according to eq 2, from which it follows that $k_1 = 2259 \pm 149$ M^{-1} s^{-1} for the coordination of hydrogen peroxide and $k_{-1} = 1.1 \pm 0.1$ s^{-1} for the back reaction. The overall equilibrium constant $K_1 = k_1/k_{-1}$ for the coordination of hydrogen peroxide at pH 8 was calculated to be 1964 ± 359 M^{-1}. It is important to note that the value of K_1 depends on the selected pH (see further Discussion).

$$k_{1obs} = k_1[H_2O_2] + k_{-1} \quad (2)$$

As a result of the $[H_2O_2]$- and pH-dependent equilibrium for the formation of the iron(III) hydroperoxo intermediate, the observed rate constant, k_{2obs}, for the formation of $\mathbf{1}^{+\bullet}$ also depends linearly on the $[H_2O_2]$ according to eq 3. The data in Figure 5 show that within experimental error a zero intercept is observed, which indicates that no back reaction occurs. From the slope of the plot, k_2K_1 was determined to be 349 ± 30 M^{-1} s^{-1} at pH 8.

$$k_{2obs} = k_2K_1[H_2O_2] \quad (3)$$

At pH 5.5 no spectrum corresponding to an iron(III)-hydroperoxo complex could be observed, but still a three exponential function was needed to obtain good fits. It is known from a previous study,[32] that the formation of iron(III)-hydroperoxo species is strongly pH dependent. At higher $[H^+]$ hydroperoxo species are not stable because of protonation and release of the hydroperoxo ligand. Presumably the same mechanism holds here. At pH 5.5 the hydroperoxo species becomes protonated, hydrogen peroxide will dissociate, and the equilibrium lies strongly to the side of **1-H_2O**. The small fraction of the iron(III)-hydroperoxo species that is formed will promptly react further to $\mathbf{1}^{+\bullet}$, and therefore $[H_2O_2]$ will

(32) Brausam, A.; van Eldik, R. *Inorg. Chem.* **2004**, *43*, 5351–5359.

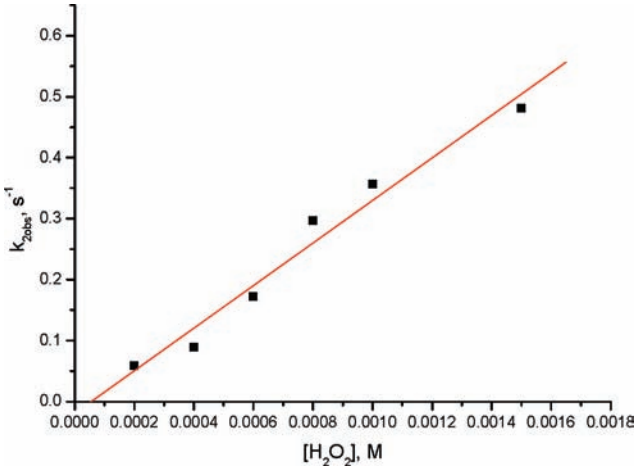

Figure 5. Plot of k_{2obs} vs $[H_2O_2]$ for the reaction of **1-H$_2$O** with hydrogen peroxide. Experimental conditions: [**1-H$_2$O**] = 1×10^{-5} M, pH 8 (0.02 M TAPS buffer), I = 0.2 M ($NaClO_4$), T = 4 °C.

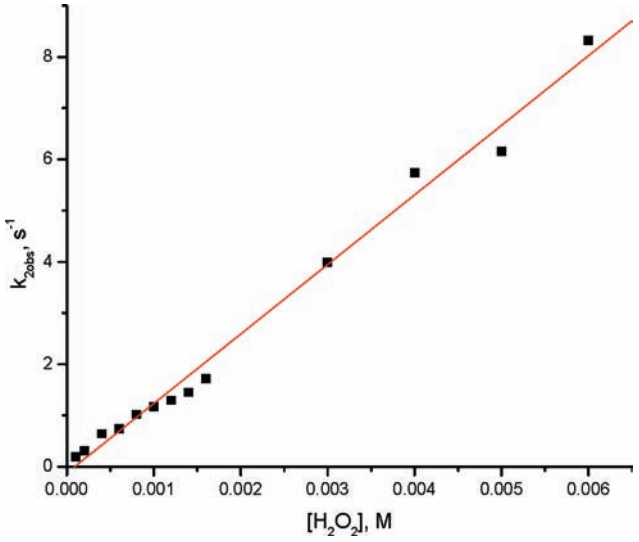

Figure 6. Plot of k_{2obs} vs $[H_2O_2]$ for the reaction of **1−OH** with hydrogen peroxide. Experimental conditions: [**1-H$_2$O**] = 1×10^{-5} M, pH 11 (0.02 M CAPS buffer), I = 0.2 M ($NaClO_4$), T = 4 °C.

have an important influence on k_{2obs}. Reliable data could only be obtained for k_{2obs} and not for k_{1obs}. k_{2obs} depends linearly on $[H_2O_2]$ according to eq 3 (Supporting Information, Figure S2) and a k_2K_1 value of 72 ± 8 M^{-1} s^{-1} at 4 °C and pH 5.5 for the formation of $\mathbf{1}^{+\bullet}$ could be calculated.

At pH > 9 the five-coordinate monohydroxo complex **1−OH** is present in solution. Kinetic data were obtained by fitting either complete spectra or kinetic traces at 488 nm. Again all kinetic data was obtained under pseudo-first-order conditions. In this pH range no spectral evidence was found for the formation of an iron(III)-hydroperoxo species. Only a single spectroscopically observable reaction, namely, the formation of $\mathbf{1}^{+}$, was observed. Best fits for the kinetic traces were obtained by using a single exponential function. At pH 11, k_{2obs} depends linearly on $[H_2O_2]$ (Figure 6).

The measured k_{2obs} is a composite value. According to Scheme 2, two kinetic models that both lead to a linear dependence of k_{2obs} on $[H_2O_2]$, are possible. The first possibility assumes a rapid pre-equilibrium with the expression for k_{2obs} given in eq 4.

$$k_{2obs} = k_2K_1[H_2O_2]/\{1+K_1[H_2O_2]\} \quad (4)$$

Only very low $[H_2O_2]$, or a small K_1 value for the coordination of hydrogen peroxide in the first reaction step, will give rise to a linear dependence of k_{2obs} on $[H_2O_2]$. At higher hydrogen peroxide concentrations, or a larger K_1 value for the formation of the Fe(III)porphyrin peroxo complex, saturation will be reached. As a result of the *trans*-labilization effect of the hydroxo group,[33] it is reasonable to expect that coordination of HOO^- is not favorable, the equilibrium constant K for the formation of the Fe(P)OOH(OH) is small, eq 4 will simplify to eq 3, and lead to a linear dependence of k_{2obs} versus $[H_2O_2]$ over the measured hydrogen peroxide concentration range. The 5-fold coordination of **1** at pH > 9 gives a further hint for the *trans*-labilization effect of the hydroxo group.

The second possible mechanism that gives rise to a linear dependence of k_{2obs} on $[H_2O_2]$ is based on the application of a steady-state approximation to Fe(P)-(OOH)(OH) in Scheme 2, for which the expression for k_{2obs} given in eq 5.

$$k_{2obs} = k_2k_1[H_2O_2]/(k_{-1}+k_2) \quad (5)$$

From the data for the binding of NO to **1**, it is known that a large intrinsic activation barrier for going from the high-spin state (S = 5/2) in **1−OH** to S = 0 in $(P^{8-})Fe^{II}$-(NO^+)(OH) is responsible for the decrease in the rate constant for the coordination of NO at high pH.[19] A similar mechanism may hold here. Upon coordination of hydrogen peroxide to **1−OH**, a change in spin state is likely to occur. Either a low spin (S = 1/2) or a spin admixed complex (P^{8-})Fe(OOH)(OH) will be formed. As a result of the coordination of H_2O_2, a change in coordination number of the Fe(III) center, its movement into the porphyrin plane and contraction of the equatorial Fe−N bonds will occur and finally lead to lower rates for the binding of hydrogen peroxide compared to the rate for homolytic cleavage of the O−O-bond to yield $\mathbf{1}^{+}$.

At present none of these possibilities can be ruled out. It is therefore not clear whether the coordination of hydrogen peroxide to **1−OH** is controlled by the lability of the Fe(III) center or by spin and structural changes upon coordination of H_2O_2 to **1−OH**. A linear fit of the data shown in Figure 6 allowed the determination of a second-order rate constant based on either eqs 3 or 5 of 1357 ± 43 M^{-1} s^{-1} at 4 °C.

k_{2obs} depends strongly on pH (Figure 7). The left part of the figure shows the pH-dependent behavior of **1-H$_2$O**, the right part that of **1−OH**. At pH < 8.5, where k_{1obs} and k_{2obs} can be separated cleanly, a slight increase in k_{2obs} with increasing pH can be observed at a given hydrogen peroxide concentration. It is known that heterolytic cleavage of the O−O-bond in iron(III)-peroxo complexes is acid catalyzed[22,34] (Scheme 1), and therefore

(33) Cusanelli, A.; Frey, U.; Richens, D. T.; Merbach, A. E. *J. Am. Chem. Soc.* **1996**, *118*, 5265–5271.
(34) Groves, J. T.; Watanabe, Y. *J. Am. Chem. Soc.* **1988**, *110*, 8443–8452.

Scheme 2. Reaction of **1−OH** with Hydrogen Peroxide

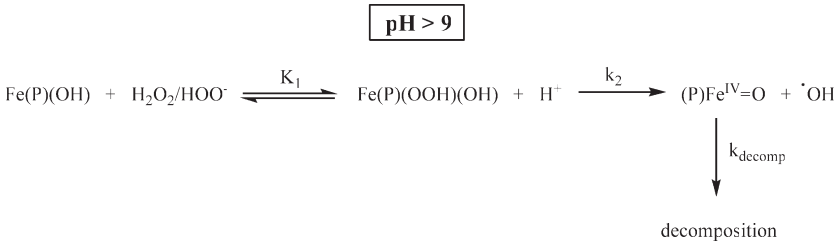

an increase in k_{2obs} should be observed. This is not the case and thus, a second dominating influence must determine the pH dependence of k_{2obs}. As mentioned above, $[H_2O_2]$ has a significant effect on k_{2obs} because of its influence on the equilibrium for the formation of the iron(III)-peroxo complex. Therefore, it is reasonable to assume that the pH-dependence for the coordination of hydrogen peroxide will influence the pH-dependence of k_{2obs}. Since coordination of hydrogen peroxide to **1-H$_2$O** affords deprotonation of the bound H_2O_2, an accelerating effect on the rate can be expected on decreasing the acid concentration. Obviously, acceleration of the coordination of H_2O_2 is the predominating one of these effects and leads to an increase in k_{2obs} with increasing pH.

For pH > 9.5 only a composite value for k_{obs} is available, which increases on increasing pH. Scheme 2 shows that only the coordination of hydrogen peroxide should be sensitive to changes in pH, since no protons or hydroxide ions are involved in the homolytic cleavage of the O−O-bond to yield $\mathbf{1}^+$. Only slight pH dependence is imaginable, if the axially bound hydroxide dissociates as water. Then the formation of $\mathbf{1}^+$ should also show slight pH dependence, namely, a decrease in rate constant with increasing pH. Presumably the predominating effect is the deprotonation of hydrogen peroxide, and therefore the pH dependence of k_{2obs} should only reflect the pH dependence of k_1 in the range 9.5−12. Again, increasing the hydoxide concentration will increase the rate of the coordination of hydrogen peroxide by facilitating deprotonation. Furthermore, at pH values around 11, deprotonated hydrogen peroxide HOO^- (pK_a = 11.3) will have an additional accelerating effect on the reaction rate. From the data points at the right side of Figure 7 the pK_a value of H_2O_2 can be determined qualitatively.

At pH > 12 all hydrogen peroxide is deprotonated, and thus no further acceleration of k_1 should be observable upon increasing pH; the slight decrease in k_{2obs} at pH > 12 is probably a result of the pH dependent decoordination of the axially bound OH^-, which should be slower at higher pH.

Pressure and Temperature Dependence of the Reaction of 1 with Hydrogen Peroxide. To determine the activation parameters $\Delta H^{\ddagger}$, $\Delta S^{\ddagger}$, and $\Delta V^{\ddagger}$ for the reaction of **1−OH** with H_2O_2 at pH 11, the kinetics were studied at different temperatures and pressures using stopped-flow techniques. Note that at this pH the activation parameters are again composite values (see eqs 3 and 5). Temperature-dependent measurements of k_{2obs} at pH 11 at a given hydrogen peroxide concentration allowed to construct an Eyring plot (Figure 8) from which $\Delta H^{\ddagger}$ = 15.0 ± 1 kJ mol^{-1} and $\Delta S^{\ddagger}$ = −128 ± 2 J K^{-1} mol^{-1} were determined. From pressure-dependent measurements $\Delta V^{\ddagger}$ could be determined to be −7 ± 1 cm^3 mol^{-1} (see Supporting Information, Figure S3).

It was not possible to determine activation parameters for the reaction of **1-H$_2$O** with hydrogen peroxide at lower pH values. Although it was still possible to observe the reaction at temperatures higher than 4 °C, it was not possible to obtain good fits to the measured kinetic traces at higher temperature. Presumably interference of the decomposition of $\mathbf{1}^{+\bullet}$ was too severe. Therefore, no

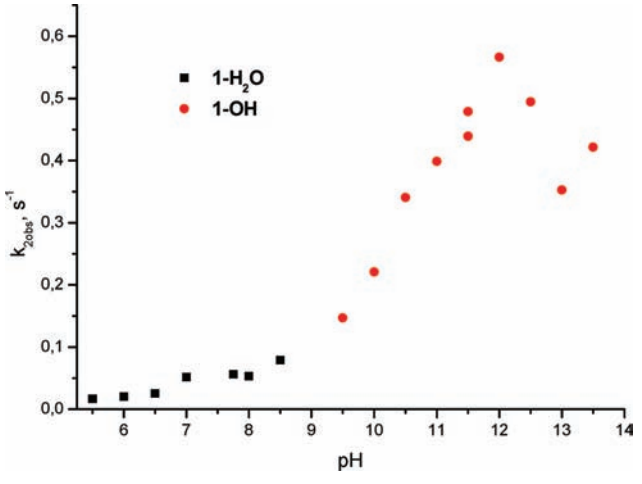

Figure 7. pH dependence of k_{2obs} for the reaction of **1** with hydrogen peroxide measured in buffered solution. pH range 5.5−13.5. Experimental conditions: [**1**] = 1 × 10^{-5} M, $[H_2O_2]$ = 2 × 10^{-4} M, I = 0.2 M ($NaClO_4$), T = 4 °C.

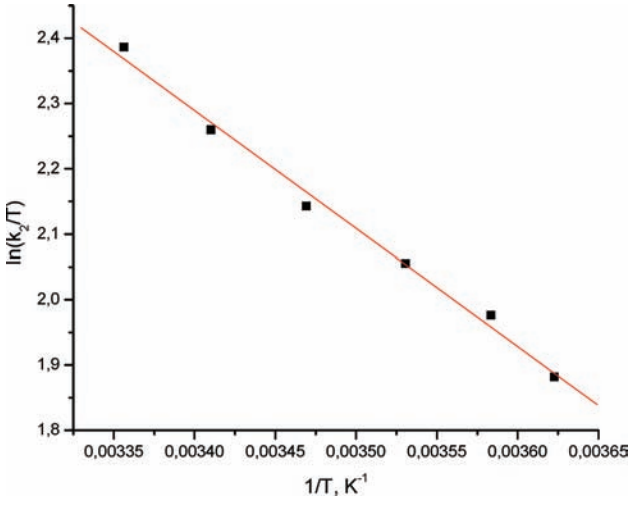

Figure 8. Eyring-Plot for k_{2obs} at pH 11. Experimental conditions: [**1−OH**] = 2 × 10^{-5} M, $[H_2O_2]$ = 2.5 × 10^{-4}, pH 11 (0.02 M CAPS buffer), I = 0.2 M.

entropy and enthalpy of activation could be reported for the reaction at low pH. As already mentioned above, kinetic traces recorded at a single wavelength at low pH values were not suitable to obtain satisfactory kinetic data. Since it is not possible to record rapid-scan spectra with the employed high pressure stopped-flow instrument as the result of a low light intensity through put, it was not possible to determine the volume of activation at low pH.

Earlier studies demonstrated that coordination of NO to **1**−**OH** follows an associatively activated mechanism. Presumably this associative reaction pathway also holds for the coordination of H_2O_2, resulting in negative values for both $\Delta S^{\ddagger}$ and $\Delta V^{\ddagger}$ for this process. Because of the electron withdrawing effect of the positively charged Fe^{III} center, the pK_a value for coordinated hydrogen peroxide is expected to be a few units below that of free hydrogen peroxide. At pH 11 the proton concentration should be much too low to efficiently protonate the coordinated OOH^- at the Fe^{III} center; therefore, no back reaction should occur and no positive contribution of the back reaction to $\Delta S^{\ddagger}$ and $\Delta V^{\ddagger}$ because of decoordination of hydrogen peroxide must be taken into account. Homolytic cleavage of the O−O bond leading to $\mathbf{1}^+$ is presumably a dissociative process. However, to estimate the overall value of $\Delta S^{\ddagger}$ and $\Delta V^{\ddagger}$ for the homolytic cleavage of the O−O-bond, it has to be taken into account that formation of $\mathbf{1}^+$ involves charge creation, which leads to negative contributions to $\Delta S^{\ddagger}$ and $\Delta V^{\ddagger}$. These two opposing effects for the homolytic cleavage of the O−O bond will presumably lead to small positive or negative values for both $\Delta S^{\ddagger}$ and $\Delta V^{\ddagger}$. In total, the composite values for $\Delta S^{\ddagger}$ and $\Delta V^{\ddagger}$ will be dominated by the associative coordination of hydrogen peroxide to **1**−**OH**.

Catalytic Oxidation of ABTS in the Presence of 1-H_2O and 1−OH. Dependence of the Rate of ABTS Oxidation on the Concentration of ABTS and 1. Upon addition of hydrogen peroxide to a solution of ABTS containing a catalytic amount of **1**, formation of the blue-green $ABTS^{+\bullet}$ radical cation (Figure 9) (Scheme 3)[35] occurs. In Figure 9 the UV/vis spectra of unreacted ABTS can be seen at wavelengths below 380 nm. Since reduced ABTS has no absorbance at wavelengths above 380 nm, it does not interfere with the kinetics measurements. Unless otherwise stated, the initial [ABTS] concentration was 0.0035 M and the concentration of **1** was 1×10^{-6} M. The reaction was monitored using stopped-flow techniques. Spectral changes for the formation of $ABTS^{+\bullet}$ were either monitored at 405 nm ($\varepsilon = 31000\ M^{-1}\ cm^{-1}$)[36] or at 660 nm ($\varepsilon = 12000\ M^{-1}\ cm^{-1}$).[35] Fits of the kinetic traces under a given condition gave identical rate constants for both wavelengths. k_{obs} values were determined by fitting the resulting kinetic traces to a single exponential function. Under the applied conditions no oxidation of ABTS was observed in the absence of **1**.

The concentration of **1** over the range 2.5×10^{-7} to 3×10^{-6} M had no significant influence on the rate of the oxidation of ABTS (see Table 1). At a given [ABTS] the oxidation of ABTS follows a pseudo-first-order reaction

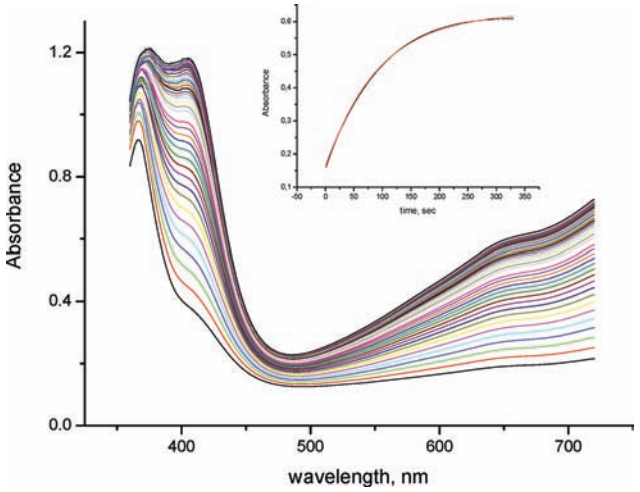

Figure 9. Spectral changes recorded for the catalytic oxidation of ABTS by H_2O_2. Experimental conditions: [**1-H_2O**] = 1×10^{-6} M, [H_2O_2] = 1×10^{-3} M, [ABTS] = 3.5×10^{-3} M, pH 8.5 (0.02 M TAPS buffer), I = 0.2 ($NaClO_4$), T = 4 °C, reaction time 330 s. Inset: single-exponential fit to the absorbance/time trace at 660 nm.

with an excess of ABTS (3.5 mM) compared to **1**, $(0.25-3) \times 10^{-6}$ M, and therefore [**1**] has no influence on the observed rate constant. It can be seen from the absorbance changes at the respective pH that at higher [**1**] more ABTS is being oxidized.

It is known from the literature that the $ABTS^{+\bullet}$ radical cation undergoes disproportionation[37,38] to give ABTS and the azodication (see Scheme 3). Accordingly unreacted ABTS stabilizes the $ABTS^{+\bullet}$ radical cation. At pH 7.4 a [ABTS]/[$ABTS^{+\bullet}$] ratio of at least 50 is required to stabilize the radical cation.[38,39] At a lower pH of 4.6 this ratio decreases to 1, indicating that disproportionation is not favored in acidic solutions.[38] These findings are supported by our own measurements of k_{obs} at various ABTS concentrations. At pH 8 variation of [ABTS] in the range from 0.0035−0.175 M had no significant influence either on the rate of ABTS oxidation, or on the yield of $ABTS^{+\bullet}$. Presumably the [ABTS] is sufficient to give a [ABTS]/[$ABTS^{+\bullet}$] ratio high enough to stabilize the radical cation. For pH 8 with [ABTS] = 0.0035 M and [**1**] = 1×10^{-6} M, this ratio equals approximately 87. At pH 8 saturation of the catalyst is reached under the applied conditions (see Supporting Information, Figure S4), and an increase in [ABTS] does not accelerate the reaction significantly, and k_{3obs} is only determined by the [H_2O_2].

At pH 11 a strong effect on both rate constant and yield was observed (Supporting Information, Figure S5). At lower concentrations up to 0.0035 M, k_{3obs} is independent of [ABTS], whereas at [ABTS] > 0.0035 M a sudden drop in the oxidation rate constant accompanied by an increase in the absorbance change for $ABTS^{+\bullet}$ is observed. As a result of the higher [ABTS], an increase in the yield of $ABTS^{+\bullet}$ is observed. The equilibrium for the disproportionation of the radical cation is shifted to the left at higher [ABTS].

(35) Huenig, S.; Balli, H.; Conrad, H.; Schott, A. *Liebigs Ann.* **1964**, *676*, 36–51.
(36) Re, R.; Pellegrini, N.; Proteggente, A.; Pannala, A.; Yang, M.; Rice-Evans, C. *Free Radic. Biol. Med.* **1999**, *26*, 1231–1237.
(37) Childs, R. E.; Bardsley, W. G. *Biochem. J.* **1975**, *145*, 92–103.
(38) Labrinea, E. P.; Georgiou, C. A. *Anal. Chim. Acta* **2004**, *526*, 63–68.
(39) Cano, A.; Hernandez-Ruiz, J.; Garcia-Canovas, F.; Acosta, M.; Arnao, M. B. *Phytochem. Anal.* **1998**, *9*, 196–202.

Scheme 3. Formation of $ABTS^{+\bullet}$ and Subsequent Disproportionation to ABTS and $ABTS^{2+}$

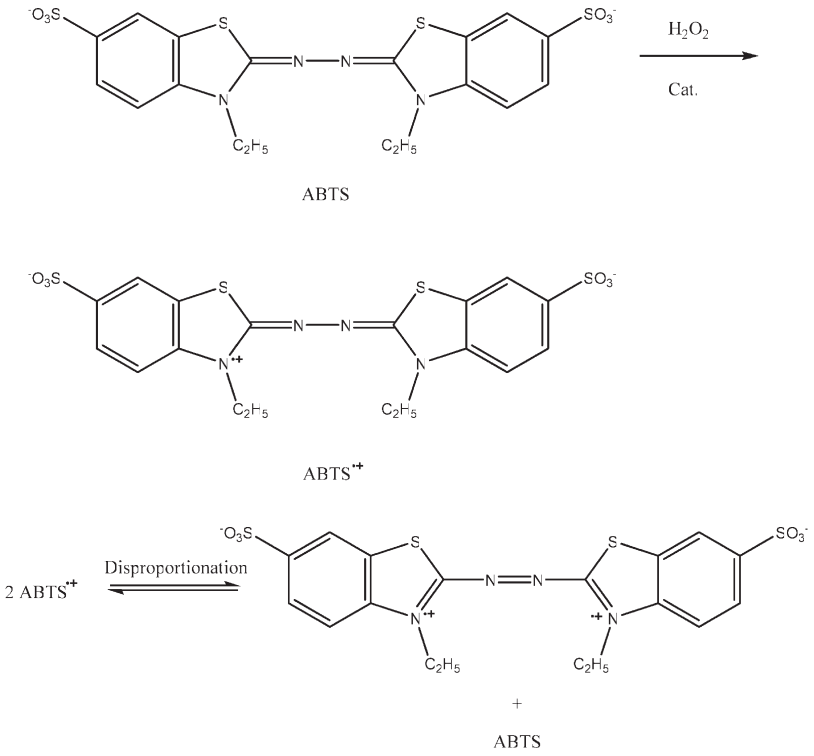

Table 1. Typical Values for k_{3obs} as a Function of Catalyst Concentration at Selected pH Values[a]

10^6 [**1**]	pH 8		pH 10		pH 11	
M	$10^3\ k_{3obs}$, s^{-1}	ΔAbs	$10^2\ k_{3obs}$, s^{-1}	ΔAbs	$10\ k_{3obs}$, s^{-1}	ΔAbs
0.25			3.0 ± 0.1	0.24		
0.5	3.4 ± 0.5	0.41	2.4 ± 0.1	0.44	1.5 ± 0.2	0.16
1.0	3.7 ± 0.1	1.23	2.80 ± 0.04	0.73	1.7 ± 0.1	0.22
2.0	3.6 ± 0.4	1.35	2.3 ± 0.4	1.12	1.3 ± 0.2	0.54
3.0			3.4 ± 0.1	1.47	1.5 ± 0.04	0.66

[a] Experimental conditions: $[H_2O_2] = 1 \times 10^{-3}$ M, [Buffer] = 0.02 M, I = 0.2 M, T = 4 °C.

Dependence of the Rate of ABTS Oxidation on $[H_2O_2]$ at Different pH. At fixed ABTS and catalyst concentrations, k_{obs} for the oxidation to the radical cation $ABTS^{+\bullet}$ shows at all investigated pH values a comparable dependence on $[H_2O_2]$. A deviation from a linear behavior is observed upon going to higher hydrogen peroxide concentrations (see Figure 10, pH 11). Depending on the pH, this deviation can be observed at $[H_2O_2] > 0.002$ at pH 6, whereas curvature at pH 11 is already evident at $[H_2O_2] > 0.0004$ M. All obtained data at the different pH could be fitted to eq 6, with k_3 representing the oxidation rate constant of ABTS. By employing an oxygen electrode it was shown that oxygen evolution occurs during the reaction. At higher peroxide concentrations both ABTS and hydrogen peroxide can react with the high valent iron oxo complex. When H_2O_2 acts as a substrate, disproportion of hydrogen peroxide occurs and leads to the formation of water and dioxygen. Thus, $k_{3catalase}$ is suggested to represent the catalase activity of **1**. The observed change in absorbance versus $[H_2O_2]$ plot (inset Figure 9) provides further evidence for the catalase activity of **1**. At low hydrogen peroxide concentrations where no catalase activity occurs, absorbance changes for the formation of $ABTS^{+\bullet}$ are constantly high, whereas at higher $[H_2O_2]$ where oxygen evolution becomes evident, a drop in absorbance for $ABTS^{+\bullet}$ is observed. The reduced peroxide concentration present in solution gives rise to a decrease in absorbance for $ABTS^{+\bullet}$, accompanied by a non-linear increase in k_{3obs} according to eq 6.

$$k_{3obs} = k_3[H_2O_2] + k_{3catalase}[H_2O_2]^2 \qquad (6)$$

From plots similar to those shown in Figure 10, k_3 and $k_{3catalase}$ could be obtained at different pH (see Table 2). The squares in Figure 10 show the measured k_{3obs} values at the respective $[H_2O_2]$, whereas the circles represent $k_{3obscal}$ that was calculated from $k_{3obs} = k_3[H_2O_2]$ using k_3 obtained from the fits according to eq 6, that is, in the absence of the catalase activity.

k_3 depends in the same way on pH as k_{2obs} for low and high pH, indicating that the reactive species responsible for the oxidation of ABTS is the high valent iron-oxo complex. Formation of $\mathbf{1}^{+\bullet}$ ($k_2K_1 = 349 \pm 30\ M^{-1}\ s^{-1}$ at pH 8 and 4 °C) and $\mathbf{1}^{+}$ (second-order rate constant from either eqs 3 or 5 of $1357 \pm 43\ M^{-1}\ s^{-1}$ at pH 11 and 4 °C) are orders of magnitude larger than k_3, providing an additional argument that the high valent oxo complexes are the catalytically active species. Turnover numbers at three different pH values were determined under conditions where neither disproportionation of $ABTS^{+\bullet}$ nor catalase activity reduced the yield of $ABTS^{+\bullet}$. Turnover numbers were calculated to be 147 at pH 6, 85 at pH 8 and 40 at pH 11. These moderate turnover numbers indicate that the catalyst **1** is not very robust and suffers from rapid degradation. The sensitivity of **1** toward self-oxidation was already assessed during measurements of the reaction of **1** with hydrogen peroxide. Addition of ABTS

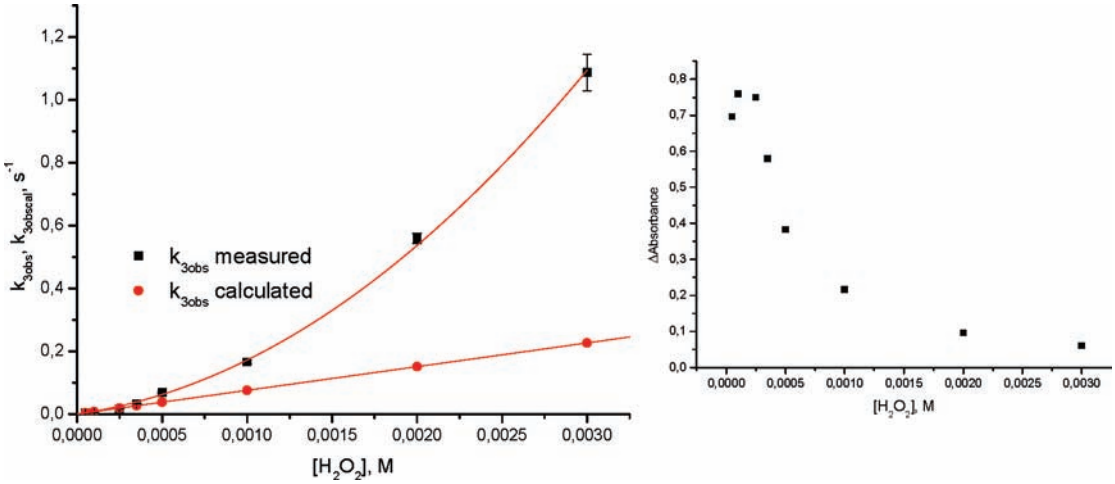

Figure 10. Plot of k_{3obs} and $k_{3obscal}$ vs $[H_2O_2]$ for the oxidation of ABTS catalyzed by **1**−**OH**. Experimental conditions: [**1**−**OH**] = 1×10^{-6} M, [ABTS] = 3.5×10^{-3} M, pH 11 (0.02 M CAPS buffer), I = 0.2 M, T = 4 °C. Inset: Plot of absorbance changes for $ABTS^{+\bullet}$ formation vs $[H_2O_2]$.

Table 2. Summary of k_3 and $k_{3catalase}$ as a Function of pH[a]

	k_3, M^{-1} s^{-1}	$k_{3catalase}$, M^{-2} s^{-1}
pH 6[b]	0.6 ± 0.1	59 ± 10
pH 8	2.7 ± 0.5	480 ± 100
pH 10	28 ± 3	6720 ± 700
pH 10.5	44 ± 24	43530 ± 8100
pH 11	76 ± 13	96500 ± 5040

[a] Experimental conditions: [**1**] = 1×10^{-6} M, $[H_2O_2] = 5 \times 10^{-5}$−$1 \times 10^{-2}$ M, [ABTS] = 3.5×10^{-3} M, pH 11 (0.02 M CAPS buffer), I = 0.2 M, T = 4°C. [b] Measured at 25 °C.

as a reducing agent could not prevent decomposition of **1**. Decomposition is also observed in the presence of a substrate and cannot be suppressed, such that the starting complex **1** can not be recovered (see also discussion of Schemes 4 and 5: Deactivation of catalyst). The relatively slow oxidation of ABTS by $\mathbf{1}^{+\bullet}$ and $\mathbf{1}^{+}$ is partially due to the competing spontaneous decomposition reactions shown in Schemes 1 and 2, and partially due to the catalase activity of these species. In addition, the high negative charge on the porphyrin will disfavor the oxidation of ABTS.

Also the degradation of the $ABTS^{+\bullet}$ radical cation depends on the concentration of hydrogen peroxide. At pH values below 10 this degradation is very slow. In acidic medium the blue-green color is observed for several hours. Above pH 10 degradation becomes faster, but since $(k_{obs})_{deg}$ for the degradation reaction is at least ten times slower then k_{3obs}, it does not interfere with the build up of $ABTS^{+\bullet}$. It seems that a certain concentration of hydrogen peroxide is necessary to have an influence on the degradation reaction (Supporting Information, Figure S6). Once this threshold is exceeded, $(k_{obs})_{deg}$ depends linearly on $[H_2O_2]$ with $k_{deg} = 19.0 \pm 0.5$ M^{-1} s^{-1} at 4 °C.

Dependence of the Rate of ABTS Oxidation on Temperature and Pressure. To determine the activation parameters $\Delta H^{\ddagger}$, $\Delta S^{\ddagger}$, and $\Delta V^{\ddagger}$ at pH 8 and 11, the kinetics for the oxidation of ABTS were studied at different temperatures and hydrostatic pressures using stopped-flow techniques. Temperature-dependent measurements of k_{3obs} at a given hydrogen peroxide concentration and pH allowed to construct Eyring plots for the respective pH value (Supporting Information, Figures S7 and S8) from which $\Delta H^{\ddagger} = 25 \pm 1$ kJ mol^{-1} and $\Delta S^{\ddagger} = -116 \pm 3$ J K^{-1} mol^{-1} at pH 11, and $\Delta H^{\ddagger} = 29 \pm 2$ kJ mol^{-1} and $\Delta S^{\ddagger} = -131 \pm 5$ J K^{-1} mol^{-1} at pH 8, were determined. From pressure-dependent measurements $\Delta V^{\ddagger}$ could be determined to be -7 ± 1 cm^3 mol^{-1} at pH 11 (Figure 11) and -2.1 ± 0.1 cm^3 mol^{-1} at pH 8 (Supporting Information, Figure S9). The overall value and sign of the activation parameters is mainly determined by charge creation upon going from ABTS to $ABTS^{+\bullet}$, resulting in negative values for the volume and entropy of activation. The slight increase in $\Delta V^{\ddagger}$ upon going from pH 11 to pH 8 is suggested to be due to intrinsic effects. At pH 11 the catalytically active compound is thought to be the Fe^{IV} species $\mathbf{1}^{+}$, whereas in contrast the catalytically active system at pH 8 is $\mathbf{1}^{+\bullet}$, formally an Fe^{V}-species. Upon oxidation of ABTS both species will be reduced to Fe^{III}. The intrinsic volume change for this reduction will be more positive at pH 8, where formally Fe^{V} is reduced to Fe^{III}. This larger positive contribution resulting from the intrinsic contribution to the overall value of $\Delta V^{\ddagger}$ for the oxidation of ABTS, reflects in a more positive value for $\Delta V^{\ddagger}$ at pH 8.

Catalytic Cycle for the Oxidation of ABTS. Scheme 4 shows the catalytic cycle for the oxidation of ABTS for pH values up to 8. Under these conditions disproportionation of $ABTS^{+\bullet}$ to ABTS and $ABTS^{2+}$ is not favored and only oxidation of ABTS to $ABTS^{+\bullet}$ has to be taken into account. On comparing the rate constants k_2 for the formation of $\mathbf{1}^{+\bullet}$ and k_3 for the oxidation of ABTS, it turns out that the oxidation of ABTS is much slower than formation of $\mathbf{1}^{+\bullet}$. This clearly indicates that $\mathbf{1}^{+\bullet}$ is the oxidizing species in the catalytic cycle (Scheme 4). Since formation of the iron peroxo complex is very fast compared to the oxidation of ABTS, the iron-peroxo complex has no chance to act as the oxidizing species. $\mathbf{1}^{+\bullet}$ is the two-electron oxidized form of **1-H$_2$O** and one molecule of H_2O_2 can oxidize two molecules of ABTS. At higher peroxide concentrations catalase activity of **1** is observed and leads to a smaller yield of $ABTS^{+\bullet}$. The lifetime of the catalyst is limited. Degradation of **1** during the reaction results in interruption of the catalytic cycle. Once **1** is deactivated, ABTS oxidation stops, although

H_2O_2 and unreacted ABTS are still present in solution. Only further addition of **1** can produce $ABTS^{+\bullet}$ again. From the direct reaction of H_2O_2 with **1-H$_2$O** it is known that deactivation involves complete destruction of the iron-porphyrin complex. Presumably $\mathbf{1}^{+\bullet}$ oxidizes itself, leading to degradation of the porphyrin ligand. An excess of substrate can not prevent the self-destruction of **1**.

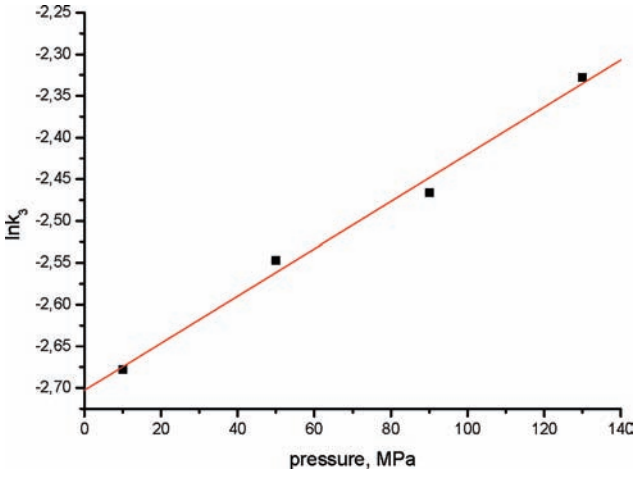

Figure 11. Plot of ln k_3 vs pressure for the catalytic oxidation of ABTS with hydrogen peroxide. Experimental conditions: [**1**−**OH**] = 1×10^{-6} M, [H_2O_2] = 3.5×10^{-4} M, [ABTS] = 3.5×10^{-3} M, pH 11 (0.02 M CAPS buffer), I = 0.2 M ($NaClO_4$), T = 25 °C.

At higher hydrogen peroxide concentrations catalase activity is observed. As a direct result of the catalase reaction the yields for $ABTS^{+\bullet}$ formation decrease although higher H_2O_2 concentrations are used. The catalase reaction consumes H_2O_2, and this causes a premature end of the oxidation reaction at higher [H_2O_2], finally leading to a non-linear increase in k_{3obs} in Figure 10.

The rate constants for formation of $\mathbf{1}^+$ and oxidation of ABTS both increase with increasing pH. At pH 11 the composite second order rate constant for the formation of the iron peroxo complex and $\mathbf{1}^+$ (1357 ± 42 M^{-1} s^{-1}) is nearly 20 times faster than k_3 (76 ± 13 M^{-1} s^{-1}) for the oxidation of ABTS, indicating that again the high valent iron oxo species **1** is responsible for the oxidation reaction. At high pH values, disproportionation of $ABTS^{+\bullet}$ must be taken into account. In strongly basic medium this disproportionation is favored and a high excess of unreacted ABTS is needed to shift the equilibrium to the left side. An ABTS concentration of 0.0035M, usually applied during this study, is not sufficient to suppress disproportionation (see Scheme 5).

Presumably OH radicals are also capable of oxidizing ABTS. In combination with the oxidizing capacity of the one-electron oxidized form $\mathbf{1}^+$, this results in a 1:2 ratio of [H_2O_2]/[ABTS] for the formation of $ABTS^{+\bullet}$.

Since oxidation of ABTS is slow, used $\mathbf{1}^+$ is permanently replaced, and then there will be a constant ratio of **1**−**OH** and $\mathbf{1}^+$. This ratio is determined by the [H_2O_2]. The total concentration of $\mathbf{1}^+$ depends on both [H_2O_2]

Scheme 4. Catalytic Cycle for the Oxidation of ABTS at Lower pH Values

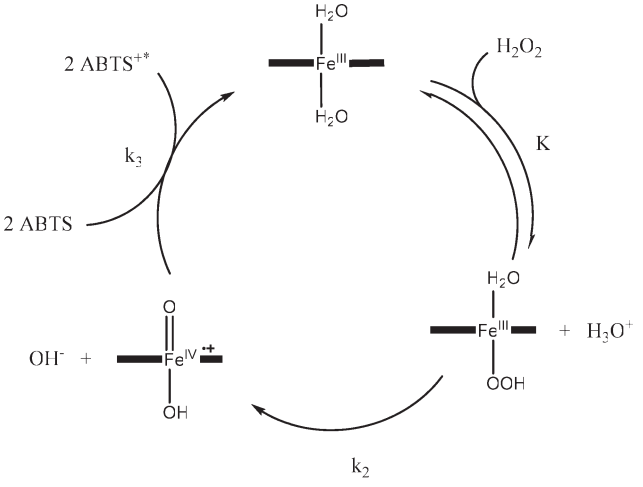

Side Reaction at high [H_2O_2]: Catalase activity

Deactivation of catalyst

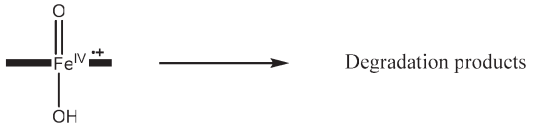

Scheme 5. Catalytic Cycle for the Oxidation of ABTS at Higher pH Values

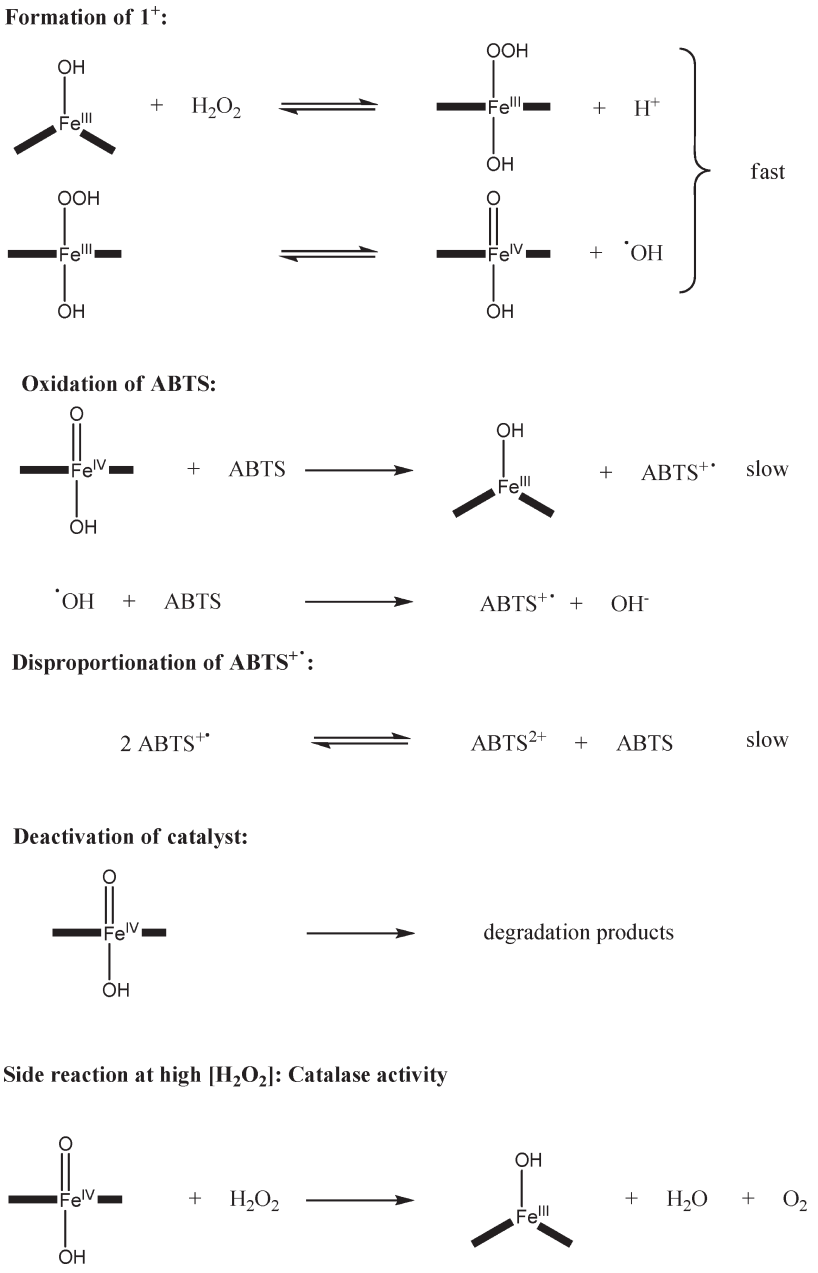

and [**1**]. As shown before, only [H_2O_2] and not [**1**] has an influence on the oxidation rate of ABTS. In the studied concentration range an increase in [**1**] does not accelerate the formation of $ABTS^{+\bullet}$.

Once $ABTS^{+\bullet}$ is formed it will disproportionate to ABTS and $ABTS^{2+}$, giving rise to a smaller absorbance change, not corresponding to the actual yield of oxidized ABTS. This disproportionation simulates a premature end of the oxidation reaction, leading to a high rate constant k_3. When a [ABTS] > 0.0035 M is used, the ratio of [ABTS]/[$ABTS^{+\bullet}$] is now high enough to stabilize the ABTS radical cation, absorbance changes for $ABTS^{+\bullet}$ are larger, the reaction can proceed to its end and finally leads to smaller rate constants k_3 as compared to lower [ABTS] (see Supporting Information, Figure S5).

At pH > 11.5 in the presence of ABTS no absorbance change for the oxidation of ABTS could be observed. Most likely the equilibrium for the disproportionation lies mainly on the side of ABTS and $ABTS^{2+}$. At higher peroxide concentrations oxygen evolution is observed again. At high pH values the catalase reaction becomes more important and oxygen evolution starts at lower [H_2O_2] as compared to only slightly basic or acidic solutions. Because of the hydrogen peroxide consumption, $ABTS^{+\bullet}$ yields drop with increasing [H_2O_2]. The decrease in yield of oxidized ABTS is accompanied by the already discussed non-linear increase in k_{3obs}.

Although $\mathbf{1}^+$ is to a certain extent more stable than $\mathbf{1}^{+\bullet}$, the lifetime of the catalyst is also limited. Again the oxidation reaction and oxygen evolution stops when the catalyst is deactivated. Excess of substrate can not prevent degradation of **1**. Upon addition of **1** the reaction starts again, and the green-blue color of $ABTS^{+\bullet}$ can be observed.

Conclusions

The results of this study clearly indicate that the nature of the high valent iron oxo species formed during the reaction of **1** with hydrogen peroxide depends on pH. At higher pH values an Fe(IV)-oxo species is formed, in contrast to lower pH values where only the Fe(IV)-porphyrin radical cation species could be observed. Under selected conditions at pH 8, rate constants for both the coordination of hydrogen peroxide and subsequent heterolytic cleavage of the O−O-bond could be obtained. At higher pH these two reaction steps could not be separated, and a composite value for the rate constant for the overall reaction to the Fe(IV)-oxo species, including coordination of hydrogen peroxide and homolytic cleavage, could be measured. Activation parameters obtained at pH 11 point to an associatively activated mechanism for the coordination of hydrogen peroxide.

Both high valent iron oxo species are not stable in aqueous solution and a total destruction of the porphyrin is observed. Both high valent iron oxo species are capable of oxidizing ABTS to the radical cation $ABTS^{+\bullet}$. The yield of this oxidation reaction is determined by both the concentration of H_2O_2 and the total concentration of unreacted ABTS in solution. Higher H_2O_2 concentrations induce catalase activity of **1**, resulting in a decrease in the yield of $ABTS^{+\bullet}$. High concentrations of ABTS present in solution disfavor disproportionation of $ABTS^{+\bullet}$ to ABTS and $ABTS^{2+}$. In acidic or only slightly basic solutions this disproportionation does not play a role.

Acknowledgment. The authors gratefully acknowledge financial support from the Deutsche Forschungsgemeinschaft within SFB 583 on "Redox-active Metal Complexes"

Supporting Information Available: Additional information as noted in the text. This material is available free of charge via the Internet at http://pubs.acs.org.